Original Research

Integrated High-Resolution Computed Tomography and Magnetic Resonance Imaging Evaluation of Temporal Bone Findings in Van der Hoeve Syndrome

Yifan Wang[1†], Xiaoqin Li[2†], Jinye Li[2], Na Hu[2], Naier Lin[1], Di Zhou[1], Qian Xi[1*], Linsheng Wang[2*]

[1] *Department of Radiology, Eye and ENT Hospital of Fudan University, Shanghai, China*

[2] *Department of Imaging Center, Shandong Second Provincial General Hospital, Jinan, China*

[*] *Corresponding authors. Qian Xi, E-mail: xiqian1129@163.com; Linsheng Wang, E-mail: jywanglinsheng@163.com*

[†] *These authors contributed equally to this work.*

© The Author(s) 2026. This article is published by Higher Education Press at journal.hep.com.cn.
This is an open access article distributed under the Creative Commons Attribution License 4.0 (CC BY), which permits unrestricted use, distribution, and reproduction in any medium, provided the original work is properly cited.

ABSTRACT

Background: Van der Hoeve syndrome (VDHS) is a rare connective tissue disorder; however, its temporal bone imaging features remain poorly characterized without integrated high-resolution computed tomography (HRCT) and magnetic resonance imaging (MRI) analysis. To address this, we systematically analyzed the imaging spectrum in a VDHS cohort using combined HRCT and MRI, and correlated these findings with clinical presentations.

Methods: Retrospective analysis of clinical, HRCT, and MRI data from eight VDHS patients (15 ears), documenting clinical manifestations along with imaging features of temporal bone and adjacent skull base.

Results: All affected ears exhibited hearing loss (tinnitus, 53.3%). All patients had blue sclerae and a history of fractures or dislocations history. Enamel hypoplasia was observed in four of the five patients with follow-up data. HRCT revealed otic capsule hypodensities in all 15 ears (target sign: eight ears), with oval window and stapes footplate involvement. On MRI, six lesions showed mild to marked enhancement (including labyrinthine enhancement). Five patients had skull base bone thinning and deformation (three with basilar invagination or platybasia).

Conclusion: The integrated HRCT and MRI assessment delineates a spectrum of temporal bone abnormalities in VDHS. When correlated with characteristic systemic manifestations, these imaging features aid in accurate diagnosis and preoperative evaluation.

KEYWORDS

Van der Hoeve syndrome, temporal bone, high-resolution computed tomography, magnetic resonance imaging

1 Introduction

Van der Hoeve syndrome (VDHS) is a rare congenital connective tissue disorder characterized by increased bone fragility due to reduced collagen, often involving multiple systems throughout the body[1,2]. It belongs to type I osteogenesis imperfecta (OI), which is the type with the mildest clinical symptoms in OI[3,4]. The main clinical manifestations of Van der Hoeve syndrome include fragile bones prone to fractures, blue sclerae, and hearing impairment[5]. In the early stage, the main clinical manifestation is a high susceptibility to fractures. In adulthood, fractures occur less frequently, and patients often seek medical attention due to hearing impairment[5].

The radiological characterization of temporal bone involvement in VDHS is not well established. Current evidence, largely derived from isolated case reports, lacks a synthesized analysis that integrates the complementary findings of high-resolution computed tomography (HRCT) and magnetic resonance imaging (MRI)[6–13]. This deficit contributes to diagnostic ambiguity, with VDHS frequently being mistaken for otosclerosis. Although the pathological relationship between the two entities remains controversial[4], a key clinical distinction

Article history: Received Aug 3, 2026; Accepted Oct 22, 2026

is widely recognized: patients with the diffuse osteopenia inherent to VDHS face a substantially greater risk of complications from stapes or cochlear implant surgery compared to otosclerosis[10,14–16]. Therefore, achieving a precise preoperative diagnosis through imaging is of critical importance.

To bridge this knowledge gap, we performed an integrated analysis of HRCT and MRI in eight patients (15 ears) with VDHS—one of the largest dedicated imaging cohorts reported. This study aims to systematically characterize the temporal bone imaging spectrum in VDHS and to demonstrate the clinical utility of this combined approach for differential diagnosis and preoperative assessment.

2 Materials and Methods

2.1 Clinical data

We retrospectively analyzed the clinical and imaging data of eight patients (15 ears) with clinically diagnosed VDHS from the electronic medical record system of the two hospitals between August 2018 and April 2025. The diagnostic criteria for VDHS in this study were formulated with reference to previous literature[17], including (1) blue sclerae, (2) fragile bones prone to fractures, (3) presence of at least one of the following: hearing impairment, tinnitus or vertigo, (4) exclusion of otosclerosis, osteitis deformans, otosyphilis, rickets, vitamin C deficiency, otitis media and bone metabolic diseases. All patients had audiological and HRCT data. MRI was performed in a subgroup of three patients (six ears) based on clinical indications. Among them, three were males and five were females. The age of the patients ranged from 21 to 55 years, with a median age of 31 years. Cochlear implantation (CI) was performed in four ears.

2.2 CT and MRI examinations

All eight patients underwent HRCT examination, using an Italian cone-beam CT system (NewTom™ 5G) or a Siemens dual-source spiral CT (SOMATOM Drive or Definition Edge, Siemens Healthineers, Forchheim, Germany). The scanning parameters were as follows. CBCT: supine position, left and right sides were scanned separately; scanning baseline: horizontal positioning line parallel to the acanthiomeatal line, voltage 110 kV, current 269.98 mA, field of view 120 mm × 80 mm, matrix 1560 × 1420, exposure time 9 s. Dual-source CT: scanning baseline was the supraorbitomeatal line, voltage 120 kV, automatic tube current modulation, collimator width 20 × 0.625 mm or 6 mm × 0.75 mm, pitch 0.6 or 0.75, field of view 190 mm × 190 mm, matrix 512 × 512, reconstruction slice thickness 0.6 mm or 0.75 mm, reconstruction interval 0.4 mm or 0.3 mm.

Three patients underwent MRI plain scan and enhanced scan, using a GE Discovery MR750w 3.0 T MR scanner with a 19-channel head and neck combined coil. Transverse T1WI fat-suppressed scanning parameters: TR 900 ms, TE 15 ms, echo train 60, matrix 256 × 256, slice thickness 1.0 mm, slice interval 0 mm, number of slices 48, field of view 205 mm × 174 mm, and number of acquisitions 2. Transverse T2WI scanning parameters: TR 2500 ms, TE 102 ms, echo train 120, matrix 256 × 256, slice thickness 1.0 mm, slice interval 0 mm, field of view 205 mm × 174 mm, number of acquisitions 2. The enhanced scan used the transverse T1WI fat-suppressed sequence, with the same parameters as above. Images were acquired immediately after intravenous injection of the contrast agent gadoteridol (Singen, Germany) at a dose of 0.2 mL/kg.

2.3 Image processing and evaluation

All original CT and MRI image data of patients were transferred from the picture archiving and communication system to the AW 4.7 workstation (GE Healthcare, Milwaukee, WI) for multiplanar reconstruction of the inner ear and auditory ossicles.

CT and MRI images were independently evaluated by two radiologists with more than 10 years of work experience. Disagreements were resolved through consultation. The clinical and temporal bone imaging (external, middle, and inner ear; ossicular chain; and adjacent skull) were recorded, including base bone density, signal intensity, and enhancement patterns. The relevant audiological classification and grading diagnostic criteria[18,19] were as follows: (1) The signal intensity of the lesion in the otic capsule area of VDHS was classified as hypointensity, slight hypointensity, isointensity, slight hyperintensity, and hyperintensity with reference to the brain parenchyma; (2) Audiological types were divided into conductive, mixed, and sensorineural deafness; (3) The degree of hearing loss was graded as mild, moderate, severe, and profound.

3 Results

3.1 Clinical manifestations of VDHS

All 15 diseased ears in eight patients had mild to profound mixed (11 ears) or sensorineural (four ears) deafness, eight ears (53.3%) were accompanied by tinnitus, and one patient (12.5%) had vertigo. All eight patients had blue sclerae (Figures 1a, 2a, and 3a), multiple fractures of the clavicle and limbs, or easy joint dislocation (Figures 1e, 2f, and 3i). Among the five followed-up patients, four had a history of enamel hypoplasia (Figures 2e and 3h). Among them, two patients patients had a family history, and four patients

underwent genetic testing, all of whom carried *COL1A1* gene mutations, as shown in Table S1.

3.2 Imaging findings of VDHS

On temporal bone HRCT, 15 ears showed patchy, strip-shaped (Figure 1b and 1c), and circular hypodensities in the otic capsule area (Figures 2b, 3b, and 3c). Among them, eight ears showed a target sign (Figures 2b, 3b, and 3c), all involving the oval window and stapes footplate, with varying degrees of thickening of the footplate (Figures 2c and 3d). Focal areas of demineralization were also noted in the ossicular chain, involving the body of the incus in four ears.

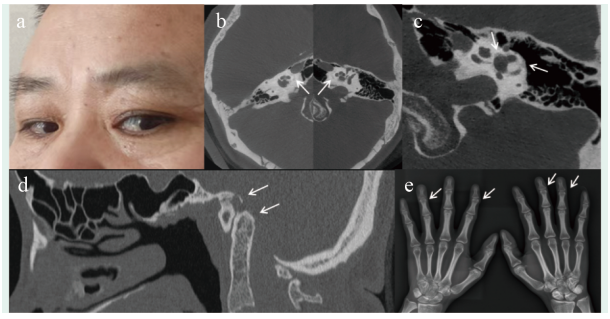


Fig. 1 Clinical and imaging features of VDHS in a representative patient. (a) Facial photograph demonstrating characteristic bilateral blue sclerae. (b–c) Axial high-resolution computed tomography (HRCT) images of the temporal bone reveal patchy and strip-shaped hypodensities (long arrows) surrounding the cochleae. (d) Sagittal HRCT reconstruction shows diffuse thinning of the skull base and basilar invagination (arrows). (e) Radiograph of the hand exhibits slender metacarpals and phalanges, cortical thinning, joint laxity, and malalignment (arrows).

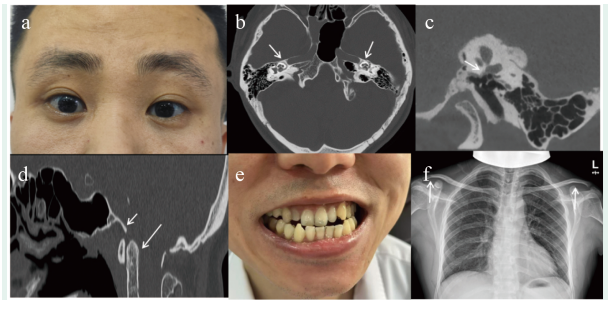


Fig. 2 Multisystem involvement in a second patient with VDHS. (a) Clinical photograph showing prominent blue sclerae. (b) Axial temporal bone high-resolution computed tomography (HRCT) demonstrates a strip-shaped hypodensity encircling the cochlea, consistent with the "target sign" (arrows). (c) Magnified HRCT view of the oval window reveals thickening and involvement of the stapes footplate (arrow). (d) Sagittal HRCT image illustrates thinning of the clivus (long arrow) and platybasia (short arrow). (e) Intraoral photograph showing enamel hypoplasia and extensive dental caries. (f) Chest radiograph depicts osteopenia, slender ribs and clavicles, and an old fractured clavicle with deformity (arrows).

On plain MRI, the above-mentioned lesions in the six otic capsule areas showed slightly prolonged T1-weighted, prolonged or slightly prolonged T2-weighted signals (Figure 3e and 3f), slight hypointensity on fluid-attenuated inversion recovery (FLAIR), mild to marked enhancement on enhanced scans, and significant enhancement in the labyrinth (Figure 3g). Among them, five patients had varying degrees of thinning and deformation of the adjacent skull base bones, and three patients were accompanied by basilar invagination or platybasia (Figures 1d and 2d).

3.3 Surgical findings

Three patients (four ears) in this group underwent CI. During the operation, it was found that the temporal bone adjacent to the electrode slot was thin and fragile, and the bone around the round window was thickened and closed, with increased fragility. The electrode was inserted carefully, and the electrode position was normal on re-examination after the operation. Facial twitching occurred in two patients after device activation, and the symptoms of facial nerve stimulation disappeared by adjusting the current. Postoperative outcomes were favorable during

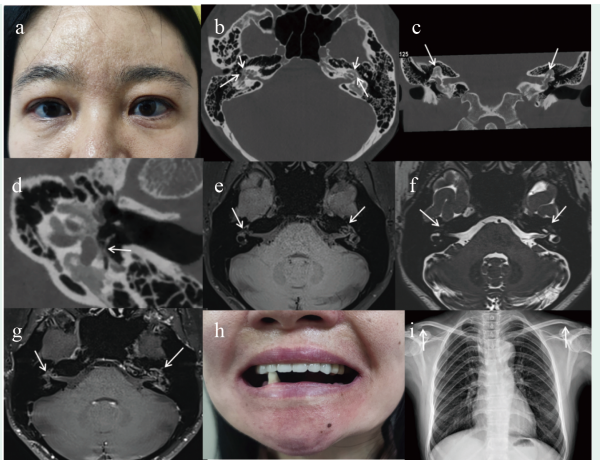


Fig. 3 Composite clinical, CT, and MRI findings in a third patient with VDHS. (a) Clinical photograph confirms blue sclerae. (b–c) Axial and coronal high-resolution computed tomography (HRCT) images of the temporal bone show extensive patchy and circumferential hypodensities (long arrows) around the cochleae, vestibules, semicircular canals, and internal auditory canals, forming a "target sign"; note concomitant thinning of the pericochlear bone (short arrows). (d) Detailed HRCT image confirms stapes footplate thickening and oval window involvement (arrow). (e–f) Axial MRI scans show lesions with mildly prolonged T1 and T2 signals within the otic capsule (arrows). (g) Contrast-enhanced fat-suppressed T1-weighted MRI shows mild to marked enhancement of the otic capsule lesions (long arrows) and marked labyrinthine enhancement (short arrows). (h) Photograph of the dentition shows severe enamel hypoplasia, caries, and loss of mandibular teeth. (i) Chest radiograph demonstrates bone thinning and a healed fracture of the clavicle with residual deformity (arrows).

follow-up.

4 Discussion

VDHS, a subtype of OI, is a rare autosomal dominant connective tissue disorder primarily caused by mutations in the *COL1A1* and *COL1A2* genes, leading to defective collagen synthesis[5]. This underlying collagen defect underlies the systemic manifestations (blue sclerae, bony fragility, dental enamel hypoplasia)[7,15] and also dictates the temporal bone pathology, which encompasses both conductive (e.g., from ossicular microfractures or stapes fixation) and sensorineural (e.g., from otic capsule demineralization or cochlear hair cell atrophy) components of hearing loss[1,13]. Patients typically present with hearing loss in young adulthood, which is progressive and often asymmetrical[4,9,12].

This study provides a systematic delineation of the temporal bone imaging spectrum in VDHS by integrating HRCT and MRI. Our findings confirm the established hallmarks, including pericochlear demineralization (frequently presenting as a "target sign"), stapes footplate thickening, and labyrinthine enhancement on post-contrast MRI[6,7,9]. Notably, the demineralization process demonstrated a potential for diffuse involvement, as evidenced by incidental focal lucency within the incus body in a subset of cases (4/15 ears). The principal diagnostic advance offered here is not a novel solitary sign, but the integrated application of this imaging spectrum. Correlating these temporal bone findings with invariant systemic features (blue sclerae, fracture history, skull base dysplasia) establishes a robust framework for reliably differentiating VDHS from isolated otosclerosis[8,9].

Consistent with and extending prior case reports[1,7,9,11,12], HRCT in our cohort revealed a spectrum of osteopenia ranging from patchy to circumferential pericochlear hypodensities. MRI complemented this by characterizing these areas with mildly prolonged T1/T2 signals and variable enhancement, often extending into the membranous labyrinth—a finding suggestive of active inflammatory or hypervascular processes[6]. Furthermore, a significant proportion of patients (5/8) exhibited concomitant thinning or deformity of the skull base, a feature that reinforces the systemic nature of the disease. It is this combination of diffuse temporal bone abnormalities and extracranial skeletal features that critically distinguishes VDHS from conditions like otosclerosis (which is focal and lacks systemic signs), Paget's disease (of older age with distinctive bone expansion), and otosyphilis (associated with specific serology and a "moth-eaten" destructive pattern)[4,10,11].

The precise radiologic identification of VDHS carries direct and significant implications for clinical management. Preoperative imaging serves as an essential roadmap: HRCT meticulously defines the extent of demineralization and identifies potential surgical obstacles such as round window atresia. Concurrently, MRI-derived markers like prominent labyrinthine enhancement may signal a state of hypervascularity, correlating with a higher observed risk of postoperative facial nerve stimulation in our and other surgical series[20]. Foreknowledge of this diffuse bony fragility and anatomic variance alerts the surgical team to the heightened risks of ossicular chain disruption and electrode misplacement, mandating tailored surgical techniques and caution.

In conclusion, our analysis underscores the definitive value of a combined HRCT and MRI approach for VDHS. HRCT excels in depicting the architectural compromise of the temporal bone, while MRI provides unique insight into associated active processes. This synergistic assessment enhances diagnostic confidence, solidifies differentiation from otosclerosis, and delivers a comprehensive anatomical overview indispensable for preoperative planning and risk stratification. The limitations of this study include its retrospective design and the small sample size inherent to rare diseases, which may affect the generalizability of findings. Future prospective studies with larger cohorts are warranted to validate the proposed imaging integration framework and further explore the debated pathological continuum between VDHS and otosclerosis.

5 Conclusion

The diagnosis of VDHS relies on a constellation of findings. Integrated HRCT and MRI of the temporal bone reveal a characteristic spectrum of abnormalities, including otic capsule demineralization, stapes footplate involvement, labyrinthine enhancement, and associated skull base dysplasia. Radiologists and otologists should be familiar with this imaging spectrum and must correlate it with the patient's systemic clinical manifestations (blue sclerae, fracture history) to achieve an accurate diagnosis, which is fundamental for appropriate patient counseling and surgical planning.

Acknowledgements

We sincerely thank all patients and colleagues for their support and collaboration.

Ethical statement

This was a retrospective study of existing clinical data. The ethical approval was granted on November 2, 2023 for Shandong Second Provincial General Hospital (Approval No. 2023-036-01), and on October 24, 2025 for Eye & ENT Hospital of Shanghai Medical School, Fudan University (Approval No. 2025245). All procedures performed were in accordance with the ethical stand-

ards of the institutional research committee and with the 1983 revision of the Declaration of Helsinki and its later amendments or comparable ethical standards.

Conflict of interest

All authors declare that they have no conflict of interest.

Funding information

This study was supported by the Shandong Medical and Health Science and Technology Development Plan (No. 202109010701).

Data availability statement

The datasets generated and analysed during the current study are not publicly available as the relevant data of this experiment are still under study. The raw data can be available from the corresponding author on reasonable request.

AI statement

The authors declare that no generative artificial intelligence (AI) or AI-assisted technologies were used in the preparation, analysis, or writing of this manuscript.

Author contributions

Yifan Wang and Xiaoqin Li contributed equally to this article. All authors contributed to the study conception and design. Material preparation, data collection and analysis were performed by Yifan Wang, Xiaoqin Li, Linsheng Wang and Qian Xi. The first draft of the manuscript was written by Yifan Wang and all authors commented on previous versions of the manuscript. All authors read and approved the final manuscript.

Supplementary files

Supplementary material is available in the online version of this article at https://doi.org/10.15302/ENTD.2026.120005 and is accessible for authorized users.

References

1. Costache A, Riza AL, Popescu M, Șerban RC, Mituț-Velișcu AM, Streață I. Diagnostic challenges in bone fragility: osteogenesis imperfecta case series. *Biomedicines*. 2025, 13(4): 865.
2. Machol K, Hadley TD, Schmidt J, et al. Hearing loss in individuals with osteogenesis imperfecta in North America: results from a multicenter study. *Am J Med Genet A*. 2020, 182(4): 697–704.
3. Panzaru MC, Florea A, Caba L, Gorduza EV. Classification of osteogenesis imperfecta: importance for prophylaxis and genetic counseling. *World J Clin Cases*. 2023, 11(12): 2604–2620.
4. Santos F, McCall AA, Chien W, Merchant S. Otopathology in osteogenesis imperfecta. *Otol Neurotol*. 2012, 33(9): 1562–1566.
5. Özen S, Gökşen D, Evin F, et al. Molecular genetic diagnosis with targeted next generation sequencing in a cohort of Turkish osteogenesis imperfecta patients and their genotype-phenotype correlation. *J Clin Res Pediatr Endocrinol*. 2024, 16(4): 431–442.
6. Alkadhi H, Rissmann D, Kollias SS. Osteogenesis imperfecta of the temporal bone: CT and MR imaging in van der Hoeve-de Kleyn syndrome. *AJNR Am J Neuroradiol*. 2004, 25(6): 1106–1109.
7. Gazzotti S, Sassi R, Aparisi Gómez MP, et al. Imaging in osteogenesis imperfecta: where we are and where we are going. *Eur J Med Genet*. 2024, 68: 104926.
8. Heimert TL, Lin DDM, Yousem DM. Case 48: osteogenesis imperfecta of the temporal bone. *Radiology*. 2002, 224(1): 166–170.
9. Hermie I, Horvath M, Van Cauter S. Temporal bone imaging features in osteogenesis imperfecta. *J Belg Soc Radiol*. 2017, 101(1): 27.
10. Kimura A, Morita Y, Kitazawa M, et al. Otic capsule demineralization and hearing outcome of stapes surgery for osteogenesis imperfecta in comparison with otosclerosis. *Otol Neurotol*. 2024, 45(5): e376–e380.
11. Renaud A, Aucourt J, Weill J, et al. Radiographic features of osteogenesis imperfecta. *Insights Imaging*. 2013, 4(4): 417–429.
12. Swinnen FKR, Casselman JW, De Leenheer EMR, Cremers CWRJ, Dhooge IJM. Temporal bone imaging in osteogenesis imperfecta patients with hearing loss. *Laryngoscope*. 2013, 123(8): 1988–1995.
13. Ziyeh S, Berger R, Reisner K. MRI-visible pericochlear lesions in osteogenesis imperfecta type I. *Eur Radiol*. 2000, 10(10): 1675–1677.
14. Nishiyama N, Kawano A, Kawaguchi S, Shirai K, Suzuki M. Cochlear implantation in a patient with Epstein syndrome. *Auris Nasus Larynx*. 2013, 40(4): 409–412.
15. Prado HV, Soares ECB, Carneiro NCR, Vilar ICDO, Abreu LG, Borges-Oliveira AC. Dental anomalies in individuals with osteogenesis imperfecta: a systematic review and meta-analysis of prevalence and comparative studies. *J Appl Oral Sci*. 2023, 31: e20230040.
16. Rotteveel LJC, Beynon AJ, Mens LHM, Snik AFM, Mulder JJ, Mylanus EAM. Cochlear implantation in 3 patients with osteogenesis imperfecta: imaging, surgery and programming issues. *Audiol Neurotol*. 2008, 13(2): 73–85.
17. Sillence DO, Senn A, Danks DM. Genetic heterogeneity in osteogenesis imperfecta. *J Med Genet*. 1979, 16(2): 101–116.
18. Cleveland C, Hayden J, Baglam T, Otteson T. Characterization of hearing loss in pediatric patients with osteogenesis imperfecta. *Int J Pediatr Otorhi*. 2024, 183: 112027.
19. Clark JG. Uses and abuses of hearing loss classification. *ASHA*. 1981, 23(7): 493–500.
20. Ugarteburu M, Cardoso L, Richter CP, Carriero A. Treatments for hearing loss in osteogenesis imperfecta: a systematic review and meta-analysis on their efficacy. *Sci Rep*. 2022, 12(1): 17125.